Contrib Mineral Petrol (1999) 134: 325–341

Friedrich Lucassen · Sven Lewerenz · Gerhard Franz
José Viramonte · Klaus Mezger

Metamorphism, isotopic ages and composition of lower crustal granulite xenoliths from the Cretaceous Salta Rift, Argentina

Received: 21 July 1998 / Accepted: 27 October 1998

Abstract Crustal xenoliths from basanitic dikes and necks that intruded into continental sediments of the Cretaceous Salta Rift at Quebrada de Las Conchas, Provincia Salta, Argentina were investigated to get information about the age and the chemical composition of the lower crust. Most of the xenoliths have a granitoid composition with quartz-plagioclase-garnet-rutile ± K-feldspar as major minerals. The exceedingly rare mafic xenoliths consist of plagioclase-clinopyroxene-garnet ± hornblende. All xenoliths show a well equilibrated granoblastic fabric and the minerals are compositionally unzoned. Thermobarometric calculations indicate equilibration of the mafic xenoliths in the granulite facies at temperatures of ca. 900 °C and pressures of ca. 10 kbar. The Sm-Nd mineral isochron ages are 95.1 ± 10.4 Ma, 91.5 ± 13.0 Ma, 89.0 ± 4.2 Ma (granitoid xenoliths), and 110.7 ± 23.6 Ma (mafic xenolith). These ages are in agreement with the age of basanitic volcanism (ca. 130–100 and 80–75 Ma) and are interpreted as minimum ages of metamorphism. Lower crustal temperature at the time given by the isochrons was above the closure temperature of the Sm-Nd system (> 600–700 °C). The Sm-Nd and Rb-Sr isotopic signatures ($^{147}Sm/^{144}Nd$ = 0.1225–0.1608; $^{143}Nd/^{144}Nd_{t0}$ = 0.512000–0.512324; $^{87}Rb/^{86}Sr$ = 0.099–0.172; $^{87}Sr/^{86}Sr_{t0}$ = 0.708188–0.7143161) and common lead isotopic signatures ($^{206}Pb/^{204}Pb$ = 18.43–18.48; $^{207}Pb/^{204}Pb$ = 15.62–15.70; $^{208}Pb/^{204}Pb$ = 38.22–38.97) of the granitoid xenoliths are indistinguishable from the isotopic composition of the Early Paleozoic metamorphic basement from NW Argentina, apart from the lower $^{208}Pb/^{204}Pb$ ratio of the basement. The Sm-Nd depleted mantle model ages of ca. 1.8 Ga from granitoid xenoliths and Early Paleozoic basement point to a similar Proterozoic protolith. Time constraints, the well equilibrated granulite fabric, *P-T* conditions and lack of chemical zoning of minerals point to a high temperature in a crust of nearly normal thickness at ca. 90 Ma and to a prominent thermal anomaly in the lithosphere. The composition of the xenoliths is similar to the composition of the Early Paleozoic basement in the Andes of NW Argentina and northern Chile. A thick mafic lower crust seems unlikely considering low abundance of mafic xenoliths and the predominance of granitoid xenoliths.

F. Lucassen (✉) · S. Lewerenz · G. Franz
Fachgebiet Petrologie, Technische Universität Berlin, Ernst-Reuter- Platz 1, EB15, D-10623 Berlin, Germany;
e-mail: luca0938@mailszrz.zrz.tu-berlin.de

J. Viramonte
Universidad Nacional de Salta, GEONORTE y CONICET, Buenos Aires 177, 4400 Salta, Argentina

K. Mezger
Mineralogisches Institut, WWU Münster, Corrensstrasse 24, D-48149 Münster, Germany

Editorial responsibility: J. Hoefs

Introduction

Complete crustal sections that expose the basement to deep levels are unknown from the Central Andes of northern Chile and NW Argentina. The last prominent orogenic cycle with high temperature (600–750 °C) low pressure (4–7 kbar) metamorphism terminated in the Devonian and caused the final exhumation of a mid-crustal section of the Early Paleozoic orogen in northern Chile and NW Argentina (Fig. 1a; Damm et al. 1990, 1994; Lucassen et al. 1996a; Becchio et al. 1997). Exposures of lower crustal rocks occur only in a small area of Sierra Limón Verde in Northern Chile (Fig. 1b). These rocks show metamorphism (*T* ca. 700 °C, *P* ca. 13 kbar) of Permian age (ca. 270 Ma) with exhumation in Early Triassic. Their isotopic composition is very similar to the composition of the Early Paleozoic metamorphic rocks that may have been their protoliths (Franz and Lucassen 1997; Lucassen et al. in press). Equivalents of these Permian lower crustal rocks are unknown.

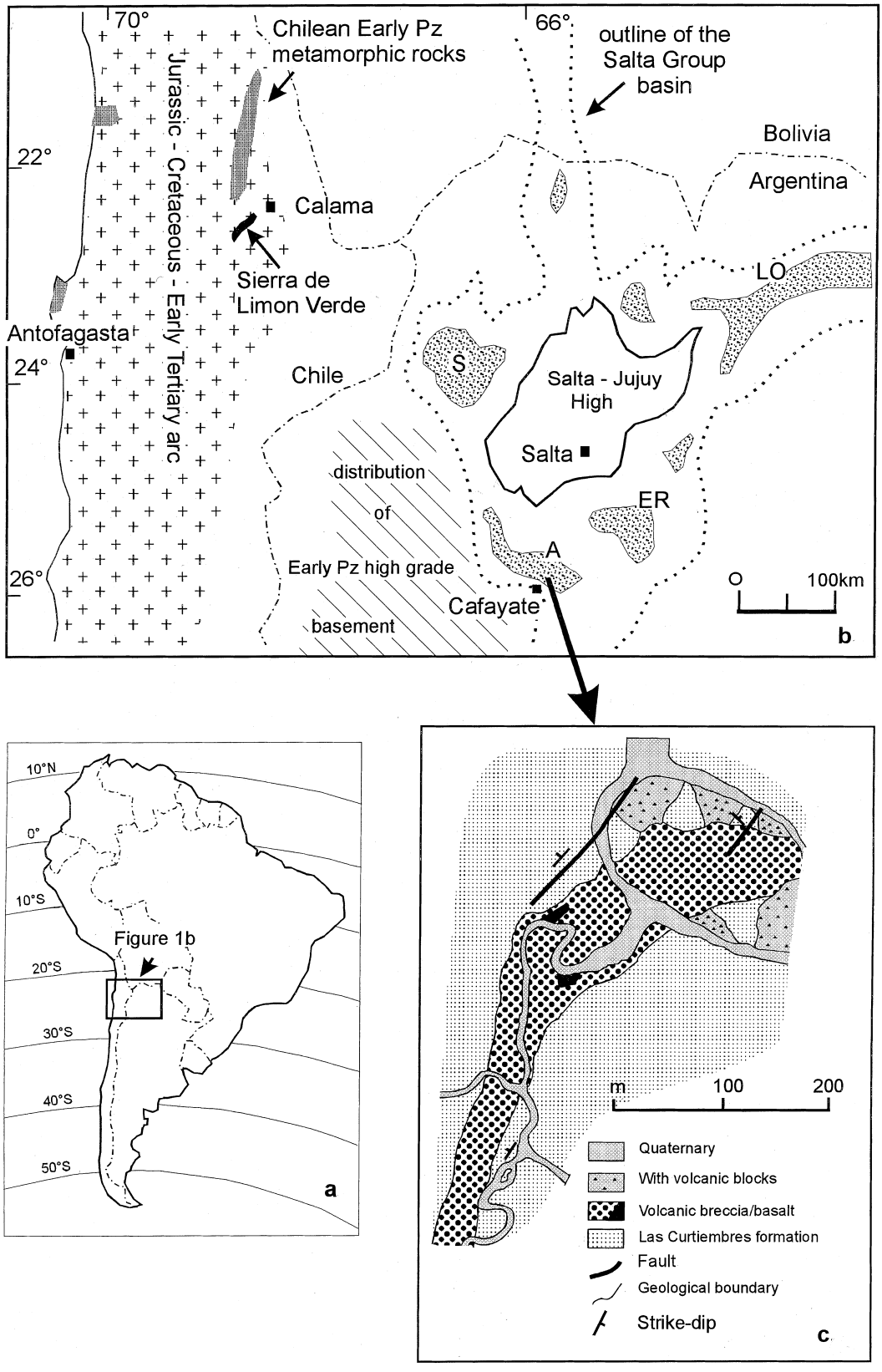
70°
66°
22°
24°
26°
Chilean Early Pz
metamorphic rocks
outline of the
Salta Group
basin
Bolivia
Argentina
Jurassic - Cretaceous - Early Tertiary arc
Calama
Sierra de
Limon Verde
Antofagasta
Chile
LO
S
Salta - Jujuy
High
Salta
distribution
of
Early Pz high grade
basement
ER
A
Cafayate
O
100km
b
10°N
0°
10°S
20°S
30°S
40°S
50°S
Figure 1b
a
m
100
200
Quaternary
With volcanic blocks
Volcanic breccia/basalt
Las Curtiembres formation
Fault
Geological boundary
Strike-dip
c

◀

Fig. 1a–c Location of the Salta Rift in South America (**a**) and outline of the Salta Group basin (**b**), showing the distribution of depocenters and morphological highs at the end of the synrift stage (modified from Fig. 5 of Salfity and Marquillas 1994). The important Cretaceous depocenters are given (*A* Alemania, *ER* El Rey, *LO* Lomas de Olmedo, *S* Sey), volcanism is restricted to the Alemania depocenter. The distribution of the Mesozoic magmatic arcs and the Early Paleozoic and Late Paleozoic (Sierra de Limón Verde) metamorphic basement is also shown. Geological sketch map of the sample area (**c**) redrawn from Koch and Lang (personal communication)

Granulite and peridotitic xenoliths (Galliski et al. 1989; Risso 1990; Risso and Viramonte 1992; Viramonte et al. in press) from the Salta Rift System (Fig. 1b; Galliski and Viramonte 1988; Salfity and Marquillas 1994) give insight into the composition and thermal structure of the lower crust in Late Cretaceous time close to the end of the active rifting. They were brought to surface by Late Cretaceous basanite volcanism in the Alemania depocentre of the Salta Group basin (Fig. 1b). These xenoliths are the only directly available samples from the deep crust of the Central Andes. Other xenoliths from volcanic rocks of the present magmatic arc are from shallow depths and comprise only sediments, volcanic rocks and metamorphic basement that are also found in outcrops.

The Central Andes are well known as the archetype of an active continental margin with a magmatic arc on a thick continental crust. The development of this magmatic arc commenced during the Late Tertiary and still continues to this day. The mechanism of crustal thickening is governed by tectonic thickening of the pre-existing continental crust. Tectonic shortening at the surface explains 70–80% of observed crustal thickening and the contributions of other processes, e.g. magmatic additions from a mantle source to the crustal thickness, seem of minor importance (review of this topic: Allmendinger et al. 1997). A cross-section through the recent Central Andes shows the overthrust of the western part onto the presumed Brazilian shield in the east interpreted from geophysical data (Fig. 2). Lithospheric delamination of old, dense continental mantle lithosphere together with dense eclogite from mafic lower crust during thickening was invoked as a process that operated in the Central Andes (Fig. 2; Kay and Kay 1993; Kay et al. 1994). Therefore, the knowledge of the pre-Tertiary compositional and thermal structure of the crust could be a valuable source of information for the interpretation of geochemical characteristics of the young volcanic rocks, large scale tectonic models and geophysical data. We present new data on the granulite xenoliths including pressure–temperature conditions

Fig. 2 Interpretation of the present lithospheric structure of the Central Andes in an E–W cross-section at ca 25°S (simplified after E. Scheuber, FU Berlin, personal communication, horizontal distance not to scale; the distance trench–sample location is ca. 500 km). The thickened crust of the Andes is thrust onto the Brazilian Shield in the east. The crustal pile of the Central Andes comprises mainly Early Paleozoic metamorphic rocks and related magmatic rocks. Mesozoic and Cenozoic additions to the crust were probably minor apart from the Jurassic–Cretaceous magmatic arc from the Coast Range to the Precordillera. The continuation of the Early Paleozoic metamorphic belt to the east is unknown. The distinction between upper and lower crust is not well constrained. Within the Brazilian Shield, stabilised during the Proterozoic, an upper and a lower (mafic?) crust are distinguished. The lithospheric delamination of the old sub-continental mantle from the east is taken from Kay et al. (1994). The *heavy dashed line* indicates a possible upper boundary of the Cretaceous upwelling of the asthenosphere

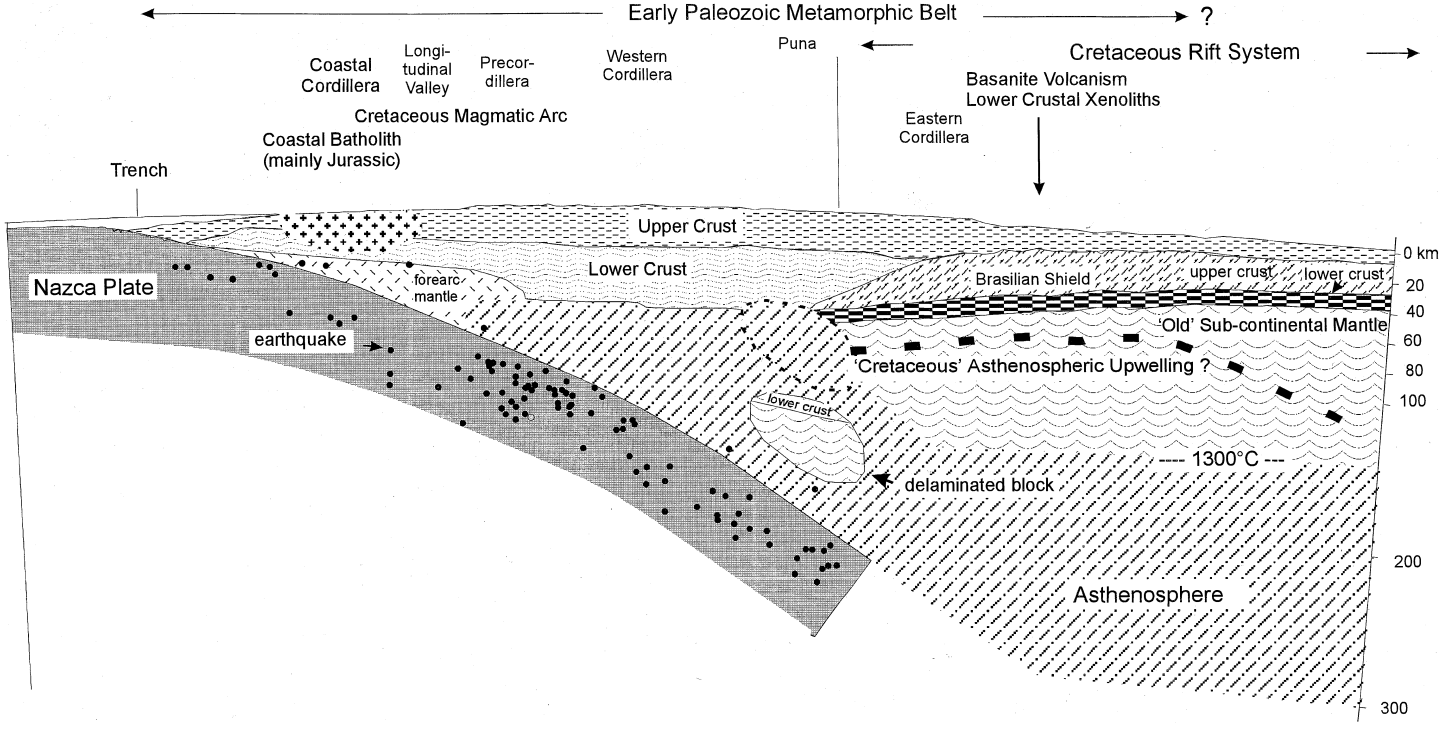

from thermobarometry, isotopic dating of minerals with the Sm-Nd system, whole rock geochemistry and isotopic systematics (Sr, Nd and Pb). A comparison of the xenoliths with the Early and Late Paleozoic metamorphic basement allows an interpretation of our findings on a more regional scale.

Geological situation

Crustal extension during the Cretaceous led to the formation of a chain of basins from NW Argentina to SW Bolivia in the Late Precambrian to Late Paleozoic basement (Fig. 1a; Galliski and Viramonte 1988; Salfity and Marquillas 1994). In NW Argentina the sediments of the Salta Group are interpreted as a rift sequence with pre-Maastrichtian (ca. 120–75 Ma) continental deposits of the synrift stage and with Maastrichtian to Eocene post-rift deposits partly of a shallow marine (?) lacustrine (?) depositional environment (Galliski and Viramonte 1988; Viramonte et al. in press). Faunal constraints on the age of the stratigraphic column are poor and age classifications of the various formations are uncertain (Salfity and Marquillas 1994). Cretaceous magmatism is of minor volume in NW Argentina and the rift could be classified as a rift of low magmatic activity (Barberi et al. 1982). However, magmatism might have been locally more important as seen in the outcrops: Modeling of the gravity field in the Lomas de Olmedo subbasin indicates mafic compositions within the strata (Fraga and Introcaso 1990). The volcanic rocks are mainly basanite to basalt. They comprise less than 5 vol.% of the Salta Group and three distinct phases of magmatism have been distinguished based on K-Ar dating, one from ca. 130–100 Ma, a second from ca. 80–75 Ma, and a third from ca. 65–60 Ma (Galliski and Viramonte 1988 and references therein). The occurrence of xenoliths seems restricted to the second volcanic pulse in the Qda. Las Conchas of the Alemania sub basin northeast of Cafayate (Fig. 1b; Galliski et al. 1989; Risso 1990; Risso and Viramonte 1992). The volcanic centres are small (a few hundred metres) and the vents are filled with breccias and intruded by small basanite dikes (m–10 m). These dikes also intruded into the sediments. Vents and dikes cut the lower parts of the late synrift Curtiembres Formation with a presumed age of < 90 Ma as the youngest sedimentary unit affected by the second volcanic pulse (Salfity and Marquillas 1994).

Xenoliths

Three main groups of xenoliths can be distinguished: *peridotites* with spinel lherzolite, harzburgite and dunite, *pyroxenite*, and *granulites* comprising granitoid and rare mafic compositions (Galliski et al. 1989; Risso 1990; Viramonte et al. in press). Granulite xenoliths are found together with pyroxenite and carbonatized peridotite in the breccia of Quebrada de Don Javier (Fig. 1c). The rounded granulite xenoliths of granitoid composition are < 30 cm in diameter and comprise $> 95\%$ of the population of crustal xenoliths, the mafic xenoliths are < 10 cm in diameter. The rocks are fresh and weathering effects are superficial.

Petrography and mineral chemistry

Contacts between the xenoliths and their host rocks are sharp and neither melting nor assimilation has been observed at the microscopic scale. Peak metamorphic mineral associations are quartz-plagioclase-garnet-rutile ± K-feldspar and kyanite in the granitoid xenoliths (samples #4-302, #4-303e, #4-304a, #A-55) and clinopyroxene-plagioclase-garnet ± hornblende in the mafic xenoliths (#4-244, #4-300, #4-301b, #A-112a). Sample #A-112b differs from both other sample types by bearing abundant garnet (ca. 50 vol.%), plagioclase and apatite (ca. 5 vol.%) and lacking quartz. Inclusions are rare to absent in all minerals. Clinopyroxene is free of exsolution lamellae. Some of the granitoid xenoliths have a compositional layering with quartz-feldspar rich and garnet rich layers. All granulites are coarse grained (ca. 1–3 mm) with a granoblastic texture and garnet porphyroblasts (< 5 mm) in some of the granitoid granulites. Pyroxene, plagioclase and quartz with curved to straight grain boundaries often form polygonal aggregates (Fig. 3). The fabric shows no preferred orientation of the minerals or formation of porphyroclasts. The grains including quartz are optically strain free. Features of dynamic recrystallization are absent and the fabric is well annealed.

Greenish to brownish kelyphitic rims occur around garnets in all samples. The width of these rims ranges from thin rinds (< 50 μm) to complete kelyphitization of the garnet. Most minerals in the kelyphitic rims are too small for microprobe analyses and it is impossible to identify any minerals except for some chlorite. Contacts between garnet and kelyphite are sharp (Fig. 3). Along grain boundaries a small greenish to clear (plain light) layer (< 10–50 μm) developed in both types of xenoliths. This layer is isotropic to microcrystalline and interpreted as former melt. Its modal proportion is below 1–2 vol.% and its major element composition is SiO_2 (~48 wt%) – Al_2O_3 (~27 wt%) – Na_2O (~10 wt%) – H_2O (ca. 12 wt% = undetermined elements) with minor CaO, K_2O, FeO and MgO (all below 2 wt%) based on microprobe analyses

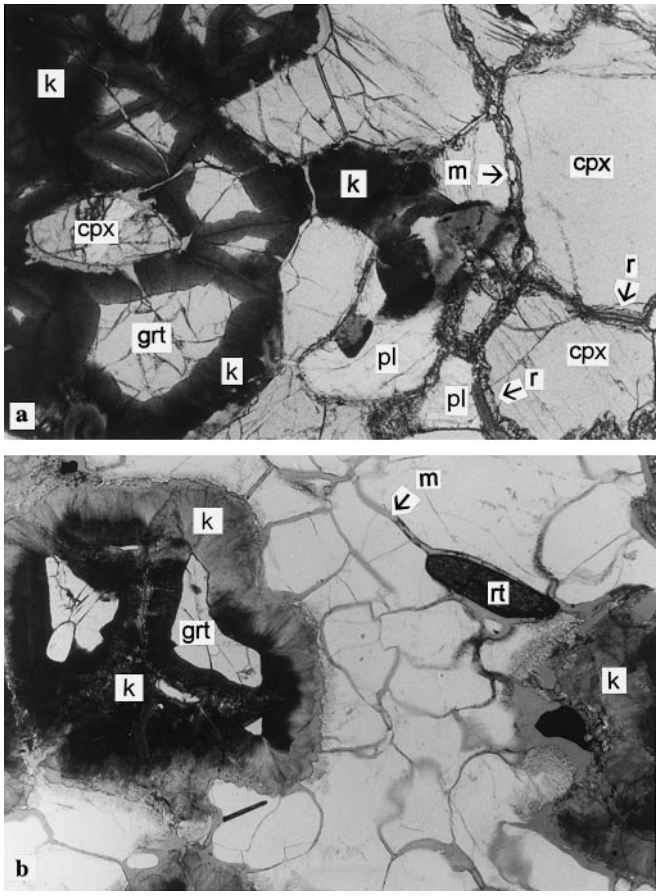

Fig. 3a,b Photomicrographs: **a** Mafic xenolith #A-112a shows kelyphitic (*k*) rim around garnet (*grt*) and kelyphitization along fractures in the garnet. Former melt (*m*) occurs along grain boundaries of plagioclase (*pl*) and clinopyroxene (*cpx*). Clinopyroxene has a rim (*r*) of secondary clinopyroxene. Plain polarised light; the *long side* of the photograph is 3.6 mm. **b** Garnet in a granitoid xenolith #4-304a shows kelyphitization. Other minerals are plagioclase and quartz (*light*) and rutile(rt). Former melt occurs along the grain boundaries. Plain polarised light; the *long side* of the photograph is 7.2 mm

(sample #A-112a; personal communication Andrea Lang). Reaction between the melt layer and plagioclase or quartz is restricted to small zones (< 10–30 μm) with the size of newly formed minerals being below the resolution of the optical microscope as well as the electron microprobe. Clinopyroxene shows a corona of secondary clinopyroxene (< 10–30 μm) with fine crystals or devitrified glass inclusions with a sharp contact to the host grain (Fig. 3). All minerals are optically unzoned apart from the reaction coronas.

Minerals of the mafic granulites were analysed to perform thermobarometric calculations (for analytical methods: see Appendix), and those of some granitoid granulites used for isotopic dating and #A-112b were checked for compositional homogeneity. All minerals were checked for zonation by analysing core and rim and were found to be unzoned. Small differences in compositions (see below) are not related to the position of the sample point in the grain but can be accounted for by the analytical uncertainty of the microprobe analysis. Grains of the same mineral species in one sample have identical compositions. Averaged compositions (Table 1) were used for each sample.

Clinopyroxenes

In the mafic granulites these are aluminous diopsides (nomenclature of Morimoto 1989) with similar compositions in the four samples. They are unzoned and no change in composition has been detected towards the reaction corona. The widest reaction rims (ca. 30 μm) developed in #A-112a. The newly formed clinopyroxene in the corona is still an aluminous diopside but has a distinct composition with higher Si, Ti, Fe, Mg and lower Al and Na (see Table 1). The Mg# [Mg/(Mg + Fe)] remains unchanged at 0.80. Similar compositional trends between clinopyroxenes from coronas and primary clinopyroxene have been described from mantle xenoliths that probably underwent partial melting and melt infiltration from the host magma during ascent (Shaw and Edgar 1997).

Hornblende

This is pargasitic (nomenclature of Leake 1978) and occurs in sample #4-244 and #4-300 of the mafic granulites.

Garnet

Garnet from the different mafic xenoliths is similar in composition and has higher pyrope and grossular and lower almandine contents than garnet from the granitoid xenoliths and the pyroxene-free mafic xenolith #A-112b (Table 1).

Plagioclase

This is rather uniform in the different mafic granulites and more variable in the granitoid xenoliths and sample #A-112b (Table 1).

Thermobarometry of the mafic granulites

Stoichiometric coefficients, activities and endmembers were calculated as required by the thermometers and barometers used. The granitoid xenoliths and #A-112b have no mineral parageneses suitable for thermobarometry. Results of thermobarometry are summarised in Table 2.

Garnet-clinopyroxene thermometry is considered to be one of the more reliable ion-exchange thermometers indicating near peak conditions due to slow diffusion in both minerals (Frost and Chacko 1989). Textural equilibrium between garnet and clinopyroxene seems well established by the granoblastic fabric and the homogeneous composition of the inclusion-free minerals. Therefore, calibration of the microprobe and precision of the measurements and their effect on Fe^{2+}-Fe^{3+} calculation remains as the major source of external uncertainties in the thermometry. Averaged mineral compositions were used for each sample in order to minimize accidental influence of the microprobe. The calibration of the garnet-clinopyroxene thermometer by Ai (1994) is the most recent among many others and it is based on a large experimental data set from different authors covering a range of P and T between 10 to 60 kbar and 600–1500 °C. Calculated mean temperatures from the four mafic xenoliths range from 830 to 920 °C. A similar temperature range from 840 to 950 °C is calculated from the hornblende-plagioclase thermometer (Holland and Blundy 1994) and garnet-hornblende thermometer (Table 2; calibrations by Graham and Powell 1984; Perchuk et al. 1985).

Garnet-clinopyroxene-plagioclase-quartz barometry (Eckert et al. 1991) and garnet-hornblende-plagioclase-quartz barometry (Kohn and Spear 1990) are based on multi-variant equilibria between the Ca and Mg endmembers of the phases. For quartz-free rocks only maximum pressures can be obtained. At a given temperature of 900 °C the calculated pressures range between 9.5 and 10.5 kbar (Table 2).

The results from the different thermometers and samples are in reasonable agreement and point to a temperature of equilibration between ca. 850 and 900 °C. The maximum pressures are also in good agreement and range from ca. 9.5–10.5 kbar for the two barometers. The occurrence of kyanite in the granitoid granulites indicates pressures > 10 kbar using the Al_2SiO_5 phase diagram of Holdaway (1971) if their temperature for equilibration was the same as for the mafic granulites. No direct proof for high temperature from thermometry was obtained but the following observations point to a high temperature equilibration of the granitoid xenoliths: fabrics including the pyrope-almandine garnet are granoblastic and the absence of zoning in the minerals records only one metamorphic stage, micas are completely absent, and the Sm-Nd isotope system in minerals of the dry rocks re-equilibrated until the time of ascent (see next section).

Sm-Nd isotopic dating, Rb-Sr and Pb isotopic composition and geochemistry

Sample selection

The Sm-Nd method was chosen for dating because of the slow diffusion of Sm-Nd and the resulting high closure temperature. This should exclude largely the effect of heating during the transport in the basanite (T ca. 1200 °C; $t \leq$ some days). Two samples from the granitoid xenoliths (#A-55, #4-304a), #A-112b, and the only mafic xenolith (#A-112a) with sufficient material for

Table 1 Electron microprobe analyses of the minerals of mafic granulite and plagioclase-quartz-garnet granulite

Plagioclase (average)

Sample	Mafic granulite				Plagioclase-quartz-garnet granulite			
	4-244	4-300	4-301b	A-112a	4-303e	4-304a	A-112b	A-55
SiO_2	57.10	55.77	56.81	54.91	61.10	63.26	59.28	67.14
Al_2O_3	27.80	28.27	27.49	28.86	24.93	24.19	24.22	20.55
FeO	0.14	0.15	0.26	0.32	0.20	0.05	0.30	0.17
CaO	9.65	10.31	9.61	10.81	6.33	5.39	6.98	0.27
Na_2O	5.88	5.58	6.11	5.32	6.98	7.69	7.06	10.69
K_2O	0.64	0.10	0.10	0.32	0.85	1.32	0.60	0.32
Total	101.33	100.26	100.46	100.62	100.51	102.12	98.51	99.32
Cations on the basis of 8 oxygens								
Si	2.534	2.502	2.539	2.460	2.705	2.755	2.686	2.948
Al total	1.455	1.495	1.448	1.524	1.301	1.242	1.294	1.064
Fe total	0.005	0.005	0.010	0.012	0.008	0.002	0.011	0.006
Ca	0.459	0.496	0.460	0.519	0.300	0.251	0.339	0.013
Na	0.506	0.486	0.530	0.462	0.600	0.649	0.620	0.910
K	0.036	0.006	0.005	0.018	0.048	0.073	0.035	0.018
Si + Al	3.99	4.00	3.99	3.98	4.01	4.00	3.98	4.01
Orthoclase	4	1	1	2	5	7	4	2
Albite	50	49	53	46	63	67	62	97
Anorthite	46	50	46	52	32	26	34	1

Hornblende (average)

Sample	Mafic granulite	
	4-244	4-300
SiO_2	42.87	42.66
TiO_2	1.76	1.52
Al_2O_3	15.40	16.58
Cr_2O_3	0.15	0.19
FeO	7.24	7.07
MnO	0.04	0.02
MgO	15.22	15.56
NiO	0.06	0.13
CaO	11.23	10.79
Na_2O	2.51	3.33
K_2O	1.52	0.40
Total	98.00	98.26
Cations on the basis of 23 oxygens		
Si	6.115	6.021
Al total	2.591	2.760
Ti	0.189	0.162
Cr	0.017	0.021
Fe total	0.864	0.834
Mn	0.005	0.003
Mg	3.236	3.274
Ni	0.007	0.015
Ca	1.716	1.632
Na	0.693	0.912
K	0.276	0.072
Total	15.702	15.706

Garnet (average)

Sample	Mafic granulite				Plagioclase-quartz-garnet granulite			
	4-244	4-300	4-301b	A-112a	4-303e	4-304a	A-112b	A-55
SiO_2	41.72	41.63	41.31	41.53	39.70	40.25	39.51	39.92
TiO_2	0.07	0.07	0.12	0.05	0.12	0.12	0.17	0.10
Al_2O_3	23.05	23.37	23.24	23.52	22.58	22.69	22.01	22.64
Cr_2O_3	0.14	0.11	0.07	–	0.04	0.05	–	–
FeO	13.68	11.68	14.57	10.42	23.13	23.06	22.83	23.89
MnO	0.34	0.26	0.37	0.23	0.49	0.46	0.46	0.47
MgO	15.87	16.97	14.99	16.62	11.13	11.58	11.40	12.37
CaO	5.83	6.08	5.98	6.62	3.02	2.16	3.49	1.12
Total	100.77	100.20	100.72	99.06	100.25	100.38	99.94	100.54

Clinopyroxene (average)

Sample	Mafic granulite				
	4-244	4-300	4-301b	A-112a	A-112a rim
SiO_2	50.84	50.14	49.89	48.82	49.54
TiO_2	0.45	0.46	0.84	0.48	1.12
Al_2O_3	7.65	8.96	7.83	9.34	5.63
Cr_2O_3	0.09	0.13	0.10	–	–
FeO	6.05	5.30	6.72	5.23	6.13
MnO	0.07	0.06	0.07	0.05	0.10
MgO	13.67	13.35	13.20	13.32	14.51
NiO	0.06	0.07	0.01	–	–
CaO	20.68	20.40	19.76	20.55	22.00
Na_2O	1.13	1.33	1.37	1.19	0.43
Total	100.69	100.20	99.80	99.00	99.59

Table 1 continued

Garnet (average)								Clinopyroxene (average)				
Sample	Mafic granulite				Plagioclase-quartz-garnet granulite				Sample	Mafic granulite			
	4-244	4-300	4-301b	A-112a	4-303e	4-304a	A-112b	A-55		4-244	4-300	4-301b	A-112a	A-112a rim
Cations on the basis of 12 oxygens									Cations on the basis of 4 cations					
Si	3.014	2.998	3.000	3.010	2.993	3.016	2.983	2.989	Si	1.846	1.823	1.830	1.795	1.829
Al total	1.963	1.984	1.990	2.010	2.007	2.005	1.959	1.998	Al total	0.327	0.384	0.339	0.405	0.245
Ti	0.004	0.004	0.007	0.003	0.007	0.007	0.009	0.006	Ti	0.012	0.013	0.023	0.013	0.031
Cr	0.008	0.006	0.004	–	0.003	0.003	–	–	Cr	0.003	0.004	0.003	–	–
Fe total	0.826	0.704	0.885	0.632	1.458	1.445	1.442	1.496	Fe total	0.184	0.161	0.206	0.161	0.193
Mn	0.021	0.016	0.022	0.014	0.031	0.029	0.029	0.030	Mn	0.002	0.002	0.002	0.002	0.003
Mg	1.709	1.821	1.623	1.795	1.251	1.293	1.282	1.380	Mg	0.740	0.723	0.722	0.714	0.793
Ca	0.451	0.470	0.465	0.514	0.244	0.173	0.283	0.090	Ni	0.002	0.002	0.000	–	–
Pyrope	57	61	54	61	42	44	48	47	Ca	0.805	0.795	0.777	0.809	0.870
Spessartine	<1	<1	1	1	1	1	1	1	Na	0.080	0.094	0.097	0.085	0.031
Grossular	15	16	15	17	8	6	3	1						
Almandine	28	23	30	21	49	49	48	50						

Table 2 Results of thermobarometry [(*1*) cpx-grt-pl-qtz barometer (Eckert et al. 1991), (*2*) grt-hbl-pl barometer (Kohn and Spear 1990),(*3*) cpx-grt thermometer (Ai 1994), (*4*) pl-hbl-(qtz) thermometry (Holland and Blundy 1994), (*5*) grt-hbl thermometer (Graham and Powell 1984)]. Abbrevations for mineral names: Kretz (1983)

Sample	[Kbar]	[°C]	Paragenesis
4/244	$9.5^{(1)}$ $10.0^{(2)}$	$880^{(3)}$ $840^{(4)}$ $840^{(5)}$	Grt-cpx-pl-hbl
4/300	$9.6^{(1)}$ $10.2^{(2)}$	$920^{(3)}$ $870^{(4)}$ $930^{(5)}$	Grt-cpx-pl-hbl
4/301b	$9.7^{(1)}$	$860^{(3)}$	Grt-cpx-pl
A/112a	$10.5^{(1)}$	$830^{(3)}$	Grt-cpx-pl

mineral separation were selected. An additional granitoid xenolith (#4-302) was analysed for whole rock isotopic compositions. The Sr isotope ratios on whole rocks and Pb isotope ratios on feldspars and whole rocks were analysed on the same samples (for sample preparation and analytical methods see Appendix).

Results of Sm-Nd dating

The Sm and Nd concentrations, Nd isotope ratios and isochron ages are listed in Table 3. Regression lines for isochrons (Fig. 4) were determined according to the method of York (1969). For MSWD > 1 errors were multiplied by the square root of the MSWD (mean squared weighted deviates). A decay constant of $6.54*10^{-12}$ a^{-1} for Sm was used. The granitoid xenoliths define isochrons with ages of 89.0 ± 4.2 Ma (#A-55) and 91.5 ± 13.0 Ma (#4-304a) including all minerals and the whole rock (Fig. 4a). The garnet-whole rock age for sample #4-304a is 94.1 ± 4.6 Ma. Sample #A-112b yields 95.1 ± 10.4 Ma using whole rock, the nonmagnetic fraction from mineral separation with REE (rare earth element) content dominated by apatite, the leached nonmagnetic fraction containing mainly plagioclase, and the garnet for isochron calculation (Fig. 4b). The garnet-whole rock age for sample #A-112b is 91.6 ± 8.3 Ma. The Sm-Nd composition of the kelyphite does not plot on the isochron and kelyphite is excluded from the regression. The mafic xenolith #A-112a has an age of 110.7 ± 23.6 Ma using kelyphitic rims, plagioclase and whole rock (Fig 4b). The three points define an isochron with MSWD = 0.0, however, the errors on the Nd ratios of whole rock and plagioclase are rather large. Clinopyroxene in sample #A-112a plots above the isochron and is not used in calculations.

The position of the clinopyroxene is probably due to the high closure temperatures for the REE diffusion in the large (diameter ca. 3 mm) clinopyroxene (Cherniak et al. 1997), and incomplete resetting during the Cretaceous heating of the rocks. An ''isochron'' with whole rock and clinopyroxene indicates ca. 420 ± 110 Ma. This ''age'' is in agreement with Sm-Nd ages of ca. 420–440 Ma from the nearby Early Paleozoic basement (Becchio et al. 1997; our unpublished data). An important part of the whole rock's Sm and Nd content is

Table 3 Sm-Nd dating and Sm-Nd whole rock composition of basanites and the average Early Paleozoic basement (*wr* whole rock, *kel* kelyphite, other mineral abbrevations, Kretz 1983)

Location/ Sample	Position	Sm[a] [ppm]	Nd[a] [ppm]	$^{147}Sm/^{144}Nd$[b]	$^{143}Nd/^{144}Nd$	Error[c]	Age[c]	Age grt-wr
4-304a wr	25°57′20″	4.557	11.14	0.2472	0.512192	0.000008	4-304a all points	
Pl	65°43′50″	1.054	7.690	0.0829	0.512120	0.000016	91.5 ± 13.0 Ma	94.1 ± 4.6 Ma
Grt		9.180	6.632	0.8370	0.512554	0.000016	Nd_i 0.512050 ± 34	
Kel		6.660	7.660	0.5250	0.512472	0.000068	MSWD = 9.8	
A55 wr		5.833	28.700	0.1225	0.512000	0.000009	A-55 all points	
Pl		0.319	2.146	0.0899	0.511995	0.000032	89.0 ± 4.2 Ma	89.2 ± 4.2 Ma
Grt		9.680	5.790	1.0090	0.512519	0.000023	Nd_i 0.511930 ± 10 MSWD = 0.7	
A-112b wr		6.317	23.748	0.1608	0.512324	0.000025	A-112b wr-pl(1)-pl(2)-grt	
Pl (1) with apatite		13.400	75.000	0.1080	0.512275	0.000009	95.1 ± 10.4 Ma	91.6 ± 8.3 Ma
Pl (2) leached		0.375	3.101	0.0730	0.512223	0.000036	Nd_i 0.512208 ± 16	
Grt		4.070	2.322	1.0620	0.512864	0.000043	MSWD = 2.3	
Kel		3.008	5.218	0.3484	0.512559	0.000012		
A-112a wr		1.781	6.685	0.1611	0.512807	0.000033	A-112a wr-pl-kel	
Pl		0.098	0.751	0.0786	0.512747	0.000072	110.7 ± 23.6 Ma	
Cpx		1.924	5.540	0.2100	0.512942	0.000014	Nd_i 0.512690 ± 50	
Kel		0.979	1.656	0.3572	0.512949	0.000015	MSWD = 0.0	
Basanites								
A-70		6.357	31.67	0.1214	0.512836	0.000033		
A-78		8.821	47.97	0.1112	0.512812	0.000010		
6-186		7.440	37.39	0.1203	0.512826	0.000031		
Average Early Paleozoic high grade basement[d]								
Weighted mean (n = 21)		5.038	24.08	0.1265	0.512057	0.000002		

[a] Measured by isotope dilution
[b] Assumed error = 0.1%
[c] Errors are 2 sigma (95% confidence level)
[d] Becchio et al. in press and our unpublished data

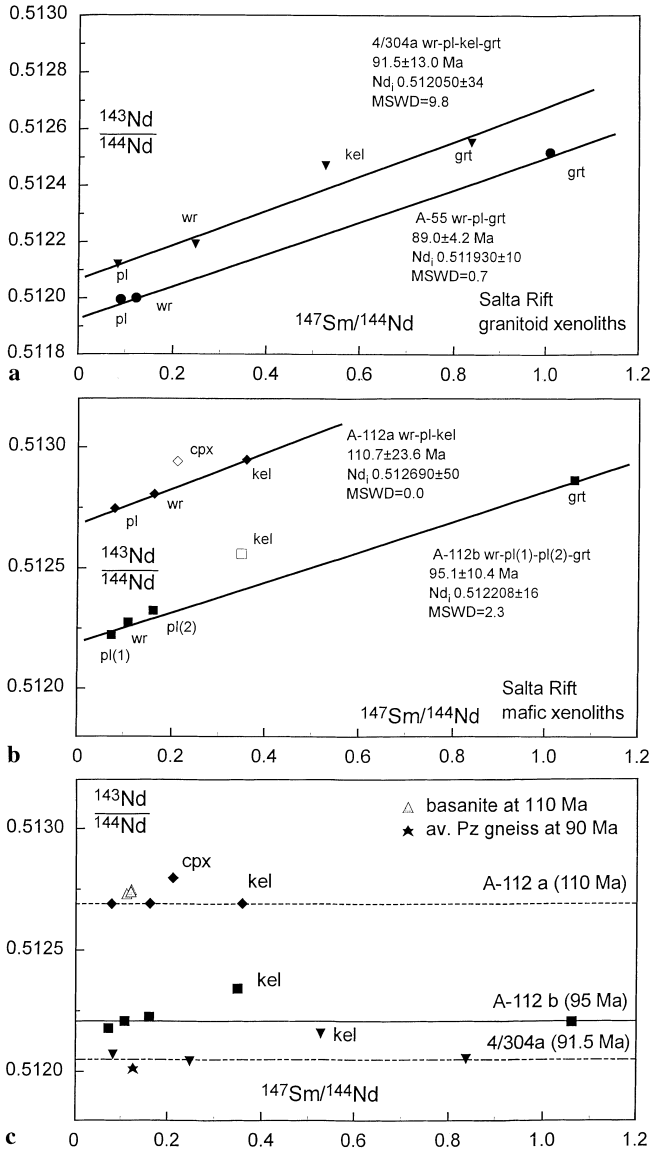

Fig. 4 Sm-Nd isochrons of granitoid (**a** #A-55 and #4-304a) and mafic (**b** #A-112a and A-112b) xenoliths (Table 2). *Pl* (*1*) and *Pl* (*2*) indicate the leached and unleached (plagioclase + apatite) fractions. All errors quoted are on the 95% confidence level (2σ). The base lines of the Sm-Nd system at the respective isochron ages for the samples containing kelyphite are shown (**c**). Sm-Nd isotopic compositions of three basanites (Table 3) at 110 Ma and of the Argentine Early Paleozoic gneisses [weighted mean ($n = 21$), Table 3; Becchio et al. in press; our unpublished data] at 90 Ma are shown as the two possible contaminants. The basanite magma is the possible contaminant of the kelyphite in samples 4-304a and A-112b, both with an isotopic composition of the whole rock similar to the average gneiss. The basanites' isotopic compositions plot close to the baseline of sample A-112a; therefore the isotopic composition of kelyphite in A-112a does not deviate from the baseline

hosted in the clinopyroxene (Table 3) that comprises ca. 50% of the mineral mode; plagioclase and kelyphite have low REE abundances. Therefore a minor mineral phase with high REE and relatively low Sm/Nd and Nd isotope ratios is needed to explain the compositional relations between clinopyroxene and whole rock. This could be a new phase that formed during Cretaceous granulite facies metamorphism with a Sm-Nd isotopic composition similar to the granitoid xenoliths or gneisses (Fig. 4c) or an old refractory phase with high closure temperature for REE and low Sm/Nd and Nd isotope ratios of possible Paleozoic age.

The Nd isotope ratios of kelyphite plot above the baseline recalculated to the respective isochron ages of samples #4-304a and #A-112b (Fig. 4c). The kelyphite is not isochemical to the garnet and contains the hydrous phase chlorite. Therefore a fluid phase must have entered from an external source. Two possible sources are the host basanites and the Paleozoic metamorphic basement (Table 3; Fig. 4c). The deviation of the kelyphite from the baseline of samples #4-304a and #A-112b could be explained by contamination with a fluid with isotopic characteristics of the basanite. The isotopic composition of kelyphite in sample #A-112a is the same as the whole rock, plagioclase and the basanites (Fig. 4c) and thus contamination by the fluid would not have changed $^{143}Nd/^{144}Nd$ of the kelyphite or the precursory garnet. If this interpretation is valid, the isochron of sample #A-112a could be real (despite the deviation of the clinopyroxene), because the garnet precursor of the kelyphite must have plotted close to the line. Therefore the garnet was in isotopic equilibrium with the plagioclase rather than the clinopyroxene. Contamination by the Paleozoic metamorphic basement seems unlikely considering its low $^{143}Nd/^{144}Nd$ ratio (Fig. 4c).

The combined Sm-Nd ages indicate that the closure of the Sm-Nd system in these rocks occurred in the Cretaceous. The three most precise isochrons (samples #4-304a, #A-55 and #A-112b) define upper Cretaceous Sm-Nd ages of ca. 90 Ma, and the poorly defined age of the mafic xenolith #A-112a is consistent with such an age, too.

Chemical and isotopic composition of the xenoliths

Granitoid samples #4-302, #4-304a and #A-55 are of similar composition (Table 4) and show similar Sr and Nd isotope ratios. The low $^{87}Rb/^{86}Sr$ ratios in all samples including the mafic rocks are common in high temperature granulite facies rocks and are interpreted to be the consequence of Rb loss (e.g. Rudnick and Presper 1990). The $^{147}Sm/^{144}Nd$ ratio of 0.24 in #4-304a is very high compared with the other granitoid samples, however its $^{143}Nd/^{144}Nd$ ratio of 0.512192 is similar.

The two mafic xenoliths are distinct from each other in their major element contents. Mineral mode in #A-112a is dominated by clinopyroxene and minor calcic plagioclase. Sample #A-112b contains sodic plagioclase and pyrope–almandine garnet in similar modal proportions; it has 0.54 wt% P_2O_5 and abundant apatite. The $^{87}Sr/^{86}Sr$ ratios in both samples are very similar with ca. 0.7081 and distinctly lower than those from the granitoid xenoliths (ca. 0.713–0.714). The $^{147}Sm/^{144}Nd$ ratios are identical with ca. 0.161 in the mafic xenoliths, but the $^{143}Nd/^{144}Nd$ ratios differ considerably with 0.512807 (#A-112a) and 0.512324 (#A-112b).

Table 4 Whole rock chemistry and isotope ratios

Sample	4-302	4-304a	A-55	A-112a	A-112b	A-112b Leached	A-112b Solution
SiO_2	61.75	60.80	65.99	47.87	45.90		
Al_2O_3	15.66	15.29	15.08	17.63	21.20		
Fe_2O_3	7.68	9.89	7.22	6.14	13.66		
MnO	0.13	0.10	0.14	0.09	0.25		
MgO	4.50	5.45	3.97	9.68	6.07		
CaO	2.19	2.25	0.96	12.03	4.00		
Na_2O	3.58	1.91	4.01	3.03	3.77		
K_2O	1.47	0.74	0.79	0.50	0.69		
TiO_2	0.99	1.18	0.87	0.83	1.73		
P_2O_5	0.05	0.04	0.07	0.07	0.54		
L.O.I.	1.81	2.20	0.58	2.35	0.83		
Total	100.00	100.02	100.11	100.04	99.05		
Ba	320	162	526	307	170		
Ga	18	12	21	14	17		
Hf	7	10	6	3	4		
Nb	16	19	21	9	24		
Rb	21	13	16	21	15		
Sc	16	13	20	56	29		
Sr	353	327	463	307	359		
V	144	139	135	137	189		
Y	32	55	65	14	60		
Zr	273	405	233	26	92		
REE[a]							
La	45	14	34	5.7	18	9.9	221
Ce	83	25	59	12	39	18	522
Pr	9.6	2.3	7.1	1.6	5.1	2.2	65
Nd	38	11	27	6.7	23	8.6	294
Sm	8.1	4.4	5.2	1.7	5.9	2.5	59
Eu	1.6	1.2	1.2	0.52	1.7	1.2	9.7
Gd	8.2	7.6	4.9	2.1	8.5	4.2	43
Tb	1.1	1.4	0.94	0.38	1.6	0.88	5.4
Dy	6	9.4	6.6	2.6	11	6.2	22
Ho	1	1.9	1.7	0.52	2.2	1.3	2.9
Er	2.8	5.6	5.9	1.6	6	3.8	5.2
Tm	0.41	0.78	0.99	0.27	0.87	0.53	0.7
Yb	2.7	5.3	6.9	1.6	5.5	3.5	2.8
Lu	0.44	0.82	1.1	0.24	0.84	0.53	0.35
La/Yb[b]	11.2	1.8	3.3	2.4	2.2	2.0	53
Nd[c]	40.370	11.140	28.700	6.685	23.748		
Sm[c]	8.790	4.557	5.833	1.781	6.317		
$^{87}Rb/^{86}Sr$	0.1716	0.1147	0.0997	0.1972	0.1205		
$^{87}Sr/^{86}Sr$ $t = 0$	0.714316	0.713142	0.713996	0.708113	0.708188		
2 sigma	0.000025	0.000025	0.000020	0.000018	0.000021		
$^{147}Sm/^{144}Nd$	0.1316	0.2472	0.1225	0.1611	0.1608		
$^{143}Nd/^{144}Nd$ $t = 0$	0.512094	0.512192	0.512000	0.512807	0.512324		
2 sigma	0.000033	0.000008	0.000009	0.000033	0.000025		
t_{DM} [Ga][d]	1.88	[−4.51]	1.85	0.94	[2.39]		
Pb isotope ratios whole rock							
$^{206}Pb/^{204}Pb$	18.4360		18.4920	18.5992	18.5645		
2 sigma	0.0017		0.0024	0.0054	0.0024		
$^{207}Pb/^{204}Pb$	15.6597		15.6642	15.6493	15.6480		
2 sigma	0.0000		0.0001	0.0002	0.0001		
$^{208}Pb/^{204}Pb$	39.6359		39.3407	38.5423	38.9916		
2 sigma	0.0002		0.0003	0.0006	0.0003		
Pb isotope ratios plagioclase							
$^{206}Pb/^{204}Pb$	18.4483	18.4797	18.4332	18.4297	18.4277		
2 sigma	0.0069	0.0026	0.0036	0.0055	0.0055		
$^{207}Pb/^{204}Pb$	15.7042	15.6559	15.6611	15.6236	15.6554		
2 sigma	0.0003	0.0001	0.0002	0.0003	0.0003		
$^{208}Pb/^{204}Pb$	39.5575	39.2039	39.1288	38.4413	39.0237		
2 sigma	0.0008	0.0003	0.0004	0.0006	0.0006		

[a] Analysed by ICP; sample A-112b leached, solution: ppm of the dry residue
[b] Calculated with normalized values
[c] Analysed by isotope dilution
[d] Model of Goldstein et al. 1984

REE distribution patterns of the granitoid samples compared with the Early Paleozoic Argentine high grade basement (Fig. 5) are similar (#4-302; La/Yb ~ 11.2), have similar L(light)REE, but higher H(heavy)REE (#A-55; La/Yb ~ 3.3) or are completely different with lower LREE and Sm enriched over Nd and higher HREE (#4-304a; La/Yb ~ 1.8).

The two mafic samples #A-112a and #A112b show distinct REE abundances, however the REE patterns are similar with La/Yb = 2.4 and 2.2. Sample #A-112b has abundant apatite and the REE patterns of the leached sample and the leach solution (Fig. 5) show the influence of the apatite on the whole rock REE abundance.

The interpretation of the deviating REE patterns and isotopic ratios of samples #4-304a and A-112b is highly speculative and no conclusions for a regional process can be drawn. The REE pattern of #4-304a could be explained in combination with its isotope ratios (Table 4; Fig. 6a). Assuming that this sample originally had a LREE pattern similar to that of the two other granitoid xenoliths, the low LREE contents could be due to a metasomatic process: garnet kept the HREE and raised the Sm/Nd ratio of sample #4-304a, whereas the LREE were preferentially removed. Accepting a metasomatic process, the similarity of the $^{143}Nd/^{144}Nd$ at 90 Ma with 0.512046 (#4-304a), 0.512016 (#4-302) and 0.511928 (#A-55) and the high $^{147}Sm/^{144}Nd$ ratio of granitoid sample #4-304a point to a Mesozoic age of this metasomatism during the granulite metamorphism. A Paleozoic or even earlier change in the $^{147}Sm/^{144}Nd$ ratio of

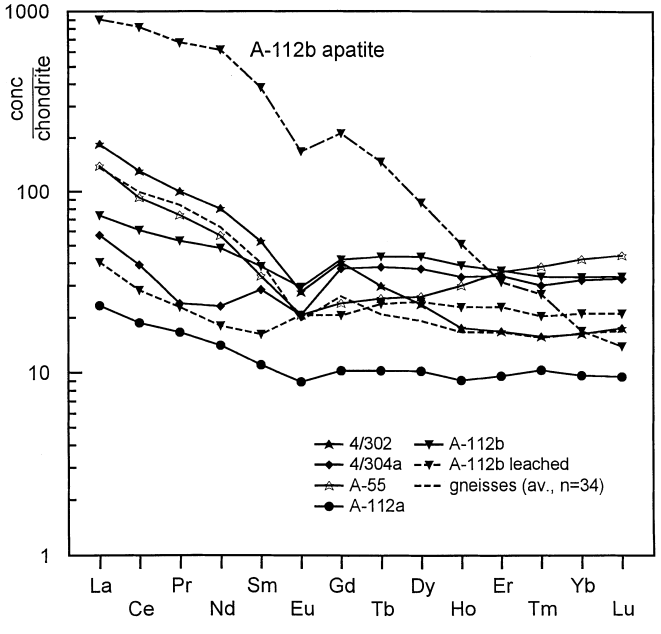

Fig. 5 REE distribution pattern of whole rock samples normalized to chondrite (Evensen et al. 1978) and comparison of the unleached and leached mafic sample #A-112b with the leach solution (Table 4). The average REE pattern of the Early Paleozoic gneisses is also shown (average of 34 samples; our unpublished data)

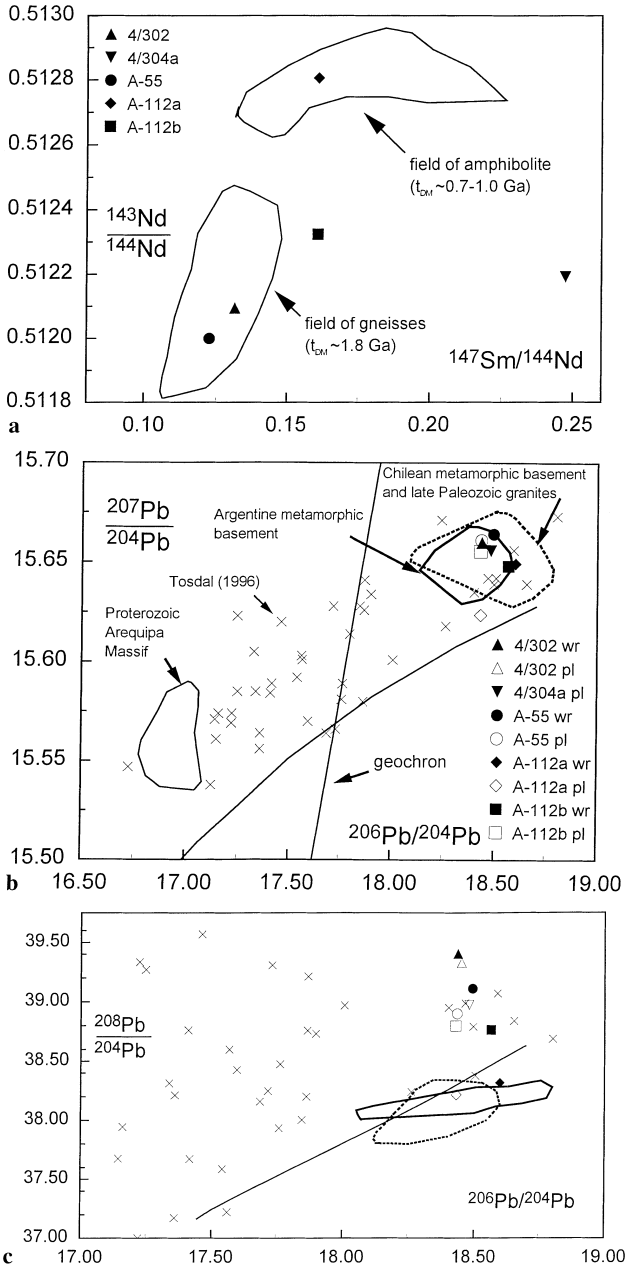

Fig. 6a–c Nd and Pb isotope ratios (Table 4): **a** Present day $^{143}Nd/^{144}Nd$-$^{147}Sm/^{144}Nd$ of xenoliths whole rock samples, compared with the field of gneisses from NW Argentina and northern Chile (n = 35; Becchio et al. in press; our unpublished data) and the field of low t_{DM} amphibolite from northern Chile (n = 12, Damm et al. 1990; Lucassen et al. in press). **b** The $^{207}Pb/^{204}Pb$-$^{206}Pb/^{204}Pb$ of xenoliths whole rock samples (*wr*) and plagioclase (*pl*) separates. The granitoid xenoliths plot into the field of the Early Palezoic–Late Paleozoic metamorphic and magmatic basement from NW Argentina and northern Chile (our unpublished data). The Paleozoic rocks and Cretaceous xenoliths plot above the average crustal lead evolution line and are in line with the development of other Proterozoic–Paleozoic basement rocks from the Central Andes (*crosses*; Tosdal 1996). Crustal lead evolution and geochron from Stacey and Kramers (1975). **c** The $^{208}Pb/^{204}Pb$ ratios of xenoliths show a broad spread compared to the Paleozoic basement rocks. Symbols as in b, solid line is the lead evolution from Stacey and Kramers (1975)

sample #4-304a would have affected the Nd isotope ratio by radiogenic growth of ^{143}Nd.

The high P_2O_5 and LREE contents of the mafic sample #A-112b could stem from an external reservoir. This reservoir had a Sm/Nd isotopic composition similar to the granitoids (Fig. 6a). The original $^{143}Nd/^{144}Nd$ isotopic ratio of #A-112b is masked by the high REE content of the apatite formed during Mesozoic metasomatism. The Sr_i isotope ratios at 90 Ma of both mafic xenoliths are very similar 0.7079 (#A-112a) and 0.7080 (#A-112b) and point to a similar source.

The Nd isotopic ratios of the unaltered xenoliths are similar to those of related rock types from NW Argentina and northern Chile (Fig. 6a). They point to a Proterozoic protolith because their depleted mantle model age (t_{DM}) of ~1.9 Ga is close to the mean value of ~1.8 Ga for the nearby Early Paleozoic low to high grade metamorphic basement of Sierras Pampeanas and Argentine Puna (Becchio et al. in press; our unpublished data). Sample #4-304a might be included in this group, but its Sm/Nd ratio has been changed probably during Cretaceous granulite metamorphism and no meaningful t_{DM} age (Table 4) could be calculated. The same argument is made for the mafic rocks: the 1.03 Ga t_{DM} of #A-112a (Table 4) is in the range of t_{DM} (ca. 0.7–1.0 Ga) from the younger group of amphibolites in northern Chile (Lucassen et al. in press), but the t_{DM} age of the metasomatically altered sample #A-112b is 2.4 Ga.

The $^{206}Pb/^{204}Pb$ and $^{207}Pb/^{204}Pb$ ratios are similar in plagioclase separates and whole rock of all xenoliths. They plot above the growth curve of average crustal Pb (Fig. 6b; Stacey and Kramers 1975), but are in the same range of values known from the gneisses and Late Paleozoic granites from northern Chile and NW Argentina (Fig. 6b; Lucassen and Franz 1997; Becchio et al. in press). The isotope ratios are in line with the growth of crustal Pb as proposed on the basis of numerous data including rocks with Grenville metamorphism by Tosdal (1996) for Bolivia and N-Chile (Fig. 6b). The $^{208}Pb/^{204}Pb$ ratios are high compared with the average growth curve and larger than in Early Paleozoic high grade metamorphic rocks in NW Argentina (Fig. 6c). The Pb isotopic composition is thus consistent with uranium depletion and an increase of the Th/U ratio as one possible process during granulite facies metamorphism (e.g. Rudnick and Presper 1990). This could have been the result of Grenvillian age metamorphism (Tosdal 1996) or Early Paleozoic ca. 500 Ma metamorphism in the Central Andes (Lucassen et al. 1996a). The scatter of $^{208}Pb/^{204}Pb$ and $^{207}Pb/^{204}Pb$ is similar to that known from the Bolivian and Peruvian Proterozoic rocks (Fig. 6b,c).

Discussion and conclusions

Metamorphic conditions

Granulite facies temperatures of 850–900 °C are well constrained for the mafic xenoliths and are in accordance with the annealed fabric. The estimated pressure of ca. 10 kbar is a maximum value because quartz is lacking in the paragenesis. The garnet-in reaction at ca. 850 °C is in the range of 7–10 kbar for SiO_2 undersaturated to saturated tholeiitic basalts (Green and Ringwood 1967; Ito and Kennedy 1971). The mineral paragenesis of granitoid xenoliths is not suitable for thermobarometry. However, granoblastic fabrics including those of the pyrope-almandine garnet, the complete absence of micas and the re-equilibration of the Sm-Nd isotope system in the dry rocks point to similar high temperatures as in the mafic xenoliths. Assuming T of ca 850 °C in the granitoid xenoliths the presence of kyanite points to a pressure of ca. 10 kbar. The fabric and the absence of zoning in the minerals record only the granulite stage and retrograde cation exchange between the minerals was not observed. The only observed reaction textures (formation of melt along grain boundaries and the formation of kelyphite) do not affect the composition of the minerals.

Age of metamorphism

The Sm-Nd mineral isochrons point to a closure of the isotope system in the Late Cretaceous at ca. 90 Ma. This age is close to ca. 130–100 and 80–75 Ma K-Ar ages of the basanitic volcanism reported from the Alemanía branch of the Cretaceous basin (Galliski et al. 1989 and reference therein). We interpret the ca. 90 Ma Sm-Nd age as the age of the entrainment of the xenoliths and instantaneous closure of the isotope system after ascent to the surface. The xenoliths were brought to surface at the end of rifting and the host basanites intruded into the uppermost synrift sediments. This implies that the lower crust at this time was still above the high closure temperatures of the Sm-Nd system (600–700 °C; Mezger et al. 1992; Thöni and Jagoutz 1992) and probably still at temperatures of granulite facies metamorphism of ca. 850–900 °C. Therefore, the Sm-Nd ages are minimum ages of the granulite metamorphism. Temperatures of 850–900 °C at 35 km depth represent a prominent thermal anomaly in the crust that continues into the mantle lithosphere. Temperatures between 1000 and 1200 °C and pressures between 13 and 15 kbar are indicated for the upper mantle from the spinel peridotite xenoliths (our unpublished data from 7 xenoliths; clinopyroxene-orthopyroxene thermometry, Brey et al. 1990; Ca in olivine barometer, Köhler and Brey 1990). This points to a continuous temperature increase with depth. We speculate that the granulite metamorphism was not a local phenomenon, e.g. the effect of contact metamorphism, but of a regional scale (Fig. 2) due to the large extent of the rift basins.

Composition of the lower crust

Chemical and isotopic compositions of the granitoid xenoliths are similar compared to those from the Early

Paleozoic metamorphic rocks and granitoids of NW Argentina (Becchio et al. in press; our unpublished data). They could be part of the Braziliano-Panafrican belt that formed during Late Precambrian–Early Paleozoic with an age of metamorphism of ca. 500 Ma (Becchio et al. 1997, in press; Lucassen et al. 1996a). Lead isotopic compositions confirm the close relation of the xenoliths to the Early Paleozoic metamorphic rocks, rather than to an old unradiogenic source such as the Arequipa Massif or Grenvillian rocks from W Bolivia (Tosdal 1996 and references therein) or the basement type found in xenoliths from the Argentine Precordillera (Kay et al. 1996). We interpret them as being part of the Early Paleozoic lower crust that resided in its position at least from the Devonian, since the Early Paleozoic orogen was already exhumed in Devonian time and no important orogenic process with crustal thickening occurred until the Tertiary formation of the Andean Plateau. The lower crust must have been already metamorphosed at granulite facies conditions before the Cretaceous overprint as indicated by the high temperature of the Early Paleozoic metamorphism known from the nearby Sierra de Quilmes and Argentine Puna (Toselli et al. 1978; Becchio et al. 1997; Lucassen et al. 1996a).

Mafic compositions comprise $< 5\%$ of the xenolith population. Both compositional types of xenoliths indicate similar metamorphic conditions; therefore they may have been collected from the same lower crustal depth. If the abundances of mafic and granitoid compositions reflect their true abundance in the lower crust then its gross composition is granitic. Admittedly this is highly speculative, since this occurrence of xenoliths is an extremely small sampling area for the lower crust. However, it is the only direct source of information, and these speculations may well serve as a guide. The only area in the Central Andes, where lower crustal rocks are exposed is at Sierra Limón Verde/northern Chile. The mafic xenolith has isotope ratios similar to mafic metamorphic rocks from this area, which presents a similarly low proportion of mafic rocks (Franz and Lucassen 1997; Lucassen et al. in press). A dominantly granitoid lower crust is in line with relatively low seismic velocities observed in the Chilean Precordillera, Altiplano and Puna [Omarini and Götze (eds) 1991; Wigger et al. 1994]. This type of lower crust is unlikely to have been involved in lithospheric delamination (Fig. 2; Kay and Kay 1993; Kay et al. 1994) because: (1) density contrasts between mantle and felsic lower crust would remain large, even at *P-T* conditions above plagioclase stability at the base of a 60 km thick crust; (2) with abundant quartz (and traces of water) present the rocks would behave ductilely. Both physical properties do not favour a mainly gravity driven separation of lower crust and descent of this lower crust attached to old continental upper mantle into the asthenosphere. If there is any major involvement of lower mafic crust in the supposed delamination process, such a crust must have formed in post–Late Cretaceous time. Promising candidates would be underplated or intruded cumulates of the Tertiary andesitic volcanism. However, the chemical signatures of the wedge derived rocks should be markedly different from those of Early Paleozoic crustal rocks with the geological history outlined above.

Cretaceous volcanism

The volcanic rocks of the Alemanía branch of the Cretaceous basin occupy only a minor volume and magmatism in NW Argentina is minor during this period. The basanites (Table 3) are of mantle origin and crustal melts are unknown (Galliski and Viramonte 1988; Galliski et al. 1989; Viramonte et al. in press), and therefore large scale melting in mantle and crust seems unlikely. Although local variations in the volume of magmatism in the different basins are observed (Fraga and Introcaso 1990), large volcanic fields are not known. This has an important implication for the composition of the lower crust and mantle lithosphere: both must have been very poor in water to avoid melting at the given high temperatures. Therefore, the Cretaceous geotherm is limited by the dry melting of granitoid and peridotite (Fig. 7). The lower crust probably had formed at granulite facies conditions already during Early Paleozoic metamorphism and was thermally overprinted during the Cretaceous.

Basin development, metamorphism and magmatism

The metamorphic–magmatic history of the Early Paleozoic orogen constrains the starting conditions of the Cretaceous sedimentation in the Salta rift system. Formation of the pre-Cretaceous crust includes deposition of the Late Proterozoic to Cambrian sediments, reorganization during Early Paleozoic high grade metamorphism and thermal and isostatic stabilization of the orogen until

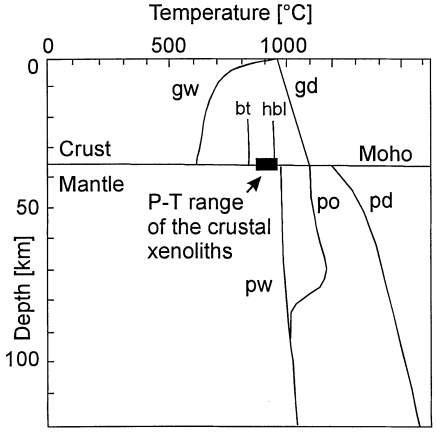

Fig. 7 Limiting thermal conditions (modified from Fig. 4.11 of Wyllie 1992) for the Salta Rift xenoliths are set by wet and dry solidi of granite; granite (*gw*; *gd*; Huang and Wyllie 1973); onset of dehydration melting of biotite (*bt*) and hornblende (*hbl*), wet and dry peridotite (*pw*, *pd*) and peridotite under oxidized (*po*) conditions

Devonian time. Subsequent changes were minor and the Cretaceous basins developed entirely on late Precambrian–Paleozoic basement (Salfity and Marquillas 1994). The basins formed between distinct morphological highs (areas without deposits) in horst-graben structures during the synrift stage (Fig. 1; for the basin development see: Marquillas and Salfity 1988; Salfity and Marquillas 1994). Sedimentation is continental throughout the synrift stage and shallow marine ingressions (?) or lacustrine deposits (?), documented in the limestones of the Yacoraite formation, are only known from the post-rift stage. Thickness of the whole Lower to Upper Cretaceous synrift succession does not exceed 2–3 km in the depocentres (age not well constrained, it could be also continental Upper Jurassic). Post-rift sediments have a maximum thickness of ca. 2.6 km, but in most parts of the basins they reach not more than ca. 1–1.5 km (Salfity and Marquillas 1994). The sedimentary infill comprises less than 15% of the presumed crustal thickness of ca. 35 km as the average value for continental crust. It is concluded from the sedimentary evolution that the crust was not substantially thinned during the Cretaceous extension and the thinning was largely compensated by sedimentation. This is in accordance with the interpretation of both the thermobarometric and age data: The xenoliths were at lower crustal depth of ca. 35 km (ca. 10 kbar) until the time of extrusion or intrusion into the stratigraphic upper unit of the synrift deposits of their host basanite at ca 90 Ma.

Contemporaneous extensional basins have a considerable N–S extension from Bolivia to Córdoba in Argentina. Basanite magmatism is also found at other locations of the rift system in Argentina (Escayola et al. in press) and Bolivia, however, its compositional and time relations are largely unknown. The distribution of the basins points to a first order process. The regional extent of the lithospheric thermal anomaly found in the Salta Rift is a matter of speculation: it could follow the Cretaceous rift basins, considering that the rift related magmatism is very minor and not necessarily traceable in all parts of the rift system. The geodynamic setting remains unclear and both a "true rift" and rifting in a possible Cretaceous back arc (Fig. 1a) have to be considered as potential scenarios.

Heat source and tectonic setting

Transport of heat by magmatic flux to the base of the crust or into the lower crust is widely accepted as a process to raise the geotherm (e.g. Wells 1980). However, there is no evidence for abundant mafic intrusions into the lower crust from the xenolith population that comprises >95% granitoids. Generation of considerable volumes of magma from a volatile poor peridotitic mantle source in the continental realm is restricted to mantle plume settings with extension and decompression above the dry solidus resulting in the production of tholeiitic flood basalts (e.g. White and McKenzie 1989) or at least large volcanic fields. Cretaceous magmatism produced only minor volumes of essentially basanitic volcanic rocks from mantle sources without magma chambers in the uppermost mantle and crust. This makes magmatic large scale underplating unlikely as the cause for the elevated geotherm. It seems possible that fusion and crystallization could have been restricted to the mantle and are not seen in the crust; the occurrence of pyroxenite xenoliths and megacrysts, that have however not yet been investigated in detail, could be an indication of this process.

Alternatively the uprise of the thermal boundary between lithosphere and asthenosphere (ca. 1300 °C; e.g. Fowler 1990) without major melting and temperatures restricted to values below the limiting geotherms in Fig. 7 can be explained by the two endmember (model) processes: heat transfer by conduction of heat only and heat transfer governed by advection of hot material (e.g. Lachenbruch and Morgan 1990; Lucassen et al. 1996b). The first transport mechanism is very slow and thermal equilibration of the lithosphere needs >100 Ma after increase of the basal heat flow at the base of the lithosphere (e.g. Fowler et al. 1988). The duration of the activity of the Cretaceous rift is not well constrained and could be ca. 20–50 Ma, considering the sedimentary record and isotopic ages of magmatism. This timespan is relatively short compared to the time needed for raising the geotherm by conduction only. For the second mechanism any tectonically forced active upwelling of hot asthenospheric material must be due to extension or another tectonic process in the mantle lithosphere only, because substantial thinning of the crust is absent. A tectonically enhanced change of the geotherm includes the uplift of the thermal boundary between lithosphere and asthenosphere (Fig. 2) by influx of hot asthenosphere into the lithospheric mantle. The high temperatures in the lower crust probably were produced by a combination of both processes, advection of heat, e.g. by the influx of hot asthenosphere, and conduction of heat that became important with ageing of the rift. The tectonic removal of possible "old sub-continental" mantle and its replacement by hot asthenosphere could also explain the sedimentary basins within horst–graben structures by thermal updoming of the normal, unthinned crust. Addition of asthenospheric material would also change the composition of the previous "old sub-continental" mantle lithosphere (Fig. 2) with consequences for the Neogene Andean volcanism. A Late Cretaceous thermal anomaly in the mantle with a possible regional extension following the rift basins must influence the thermal structure and therefore the rheological properties of the lithosphere throughout the Tertiary, because re-equilibration is so slow. The thorough study of mineral phases and chemistry of rift related volcanic rocks and mantle xenoliths will be necessary to prove this model.

Acknowledgements The research of this paper is a result of Sfb 267 "Deformation Processes in the Andes". We thank the Deutsche Forschungsgemeinschaft for financial support and grant L-501/2 to F.L. We thank CIUNSa (Consejo de Investigaciones de la

Universidad Nacional de Salta) for supporting this research. Andrea Lang and Kerstin Koch, TU Berlin, contributed samples and the geological map of Qda. Don Javier from their diploma theses. We thank Heidi Baier and Sigmund Rochnowski (both Münster) for help with the isotope analyses, Maren Krause for preparation of the REE determinations at GeoForschungsZentrum, Potsdam, and François Galbert for help with the microprobe at ZELMI, TU Berlin. Reviews by Kurt Mengel and Heinz-Günter Stosch are gratefully acknowledged.

Appendix: analytical methods

Mineral compositions were obtained using an automated CAMEBAX microprobe (at TU Berlin) at 15 kV acceleration voltage and 20 nA sample current. For correction the ZAF and PAP programs were used. The electron beam was focused to < 5 μm except for plagioclase which was measured with a 5 μm beam. Standards used are potassic feldspar for K, albite for Na, wollastonite for Ca, andalusite for Si and Al, rutile for Ti, olivine for Mg, pure metals for Fe, Mn, Cr, and Ni.

Minerals were separated using a magnetic separator followed by handpicking under the binocular microscope. Clinopyroxene, garnet and the non-magnetic fraction of #A-112b (the latter contained abundant apatite) were leached for 20 minutes in 2n HCl in order to remove apatite. Separation of a sufficient volume of garnet from #A-112a was impossible due to the small sample size and the low abundance of garnet. After dissolution bulk REE were separated by conventional cation exchange. For the whole rock samples the Sr fraction was eluted from the same aliquot and separated from Rb by standard cation-exchange technique. The Nd-Sm were separated using quartz glass columns with Teflon powder coated with HDEHP (Richard et al. 1976). The Nd was eluted using 0.17n HCl, followed by Sm in 0.4n HCl. Both Sr and Nd isotope ratios and Sm and Nd concentrations were measured on a VG Sector 54 mass spectrometer at the Zentrallaboratorium für Geochronologie Universität Münster. During the time of measurement the La Jolla Nd standard yielded a $^{143}Nd/^{144}Nd = 0.511835 \pm 4$ (2σ; $n = 10$). An external precision (reproducibility) of 0.1% is assumed for the $^{147}Sm/^{144}Nd$ ratio from the Sm-Nd concentrations by the isotope dilution technique. The Nd isotope ratios were normalized to $^{146}Nd/^{144}Nd = 0.72190$. The Sr standard NBS 987 yielded $^{87}Sr/^{86}Sr = 0.710261 \pm 11$ (2σ; $n = 4$) during the course of the measurements.

Lead isotope ratios were determined on four feldspar separates, the corresponding whole rock samples and whole rock sample # 4-302. Feldspars were leached in HF and HNO_3 before final dissolution in order to remove possible radiogenic Pb (DeWolf and Mezger 1994). Lead was separated by standard ion exchange using HBr and HCl chemistry. The Pb standard NBS981 yielded $^{204}Pb/^{206}Pb = 0.05923 \pm 5$, $^{207}Pb/^{206}Pb = 0.91345 \pm 18$, $^{208}Pb/^{206}Pb = 2.1614 \pm 4$ (2σ; $n = 5$) during the course of the measurements. Lead isotope ratios from all samples were corrected for fractionation based on the values for the NBS standard SRM981.

Major and trace element contents of the five xenoliths were determined by XRF on fused glass disks at TU Berlin using Oxiquant and X-40 Philips software. The REE contents were determined by ICP-AES at the GFZ Potsdam (Zuleger and Erzinger 1988).

References

Ai Y (1994) A revision of the garnet-clinopyproxene Fe^{2+}-Mg exchange geothermometer. Contrib Mineral Petrol 115: 467–473

Allmendinger W, Jordan TE, Kay SM, Isacks BL (1997) The evolution of the Altiplano–Puna plateau of the Central Andes. Annu Rev Earth Planet Sci 25: 139–174

Barberi F, Santacroce R, Varet J (1982) Chemical aspects of rift magmatism: continental and ocean rifts. Geodyn Ser 8: 223–258

Becchio R, Lucassen F, Franz G, Viramonte J (1997) Condiciones de *P-T* del basamento metamorfico de alto grado, borde oriental de la Puna Austral, Argentina. VIII Congr Geol Chileno, Antofagasta, Chile, Actas Vol II: 1220–1224

Becchio R, Lucassen F, Franz G, Viramonte J, Kasemann S (1998) Geoquimica del basamento de la Puna Austral y Cordillera Oriental. X Congr Latinoamericano Geol, Buenos Aires, Actas (in press)

Brey GP, Köhler T, Nickel KG (1990) Geothermobarometry in four-phase lherzolites II. Experimental results from 10 to 60 kbar. J Petrol 31: 1313–1352

Cherniak DJ, Hanchar JM, Watson EB (1997) Rare-earth diffusion in zircon. Chem Geol 134: 289–301

Damm KW, Pichowiak S, Harmon RS, Todt W, Kelley S, Omarini R, Niemeyer H (1990) Pre-Mesozoic evolution of the central Andes; the basement revisited. In: Kay SM, Rapela CW (eds) Plutonism from Antarctica to Alaska. Geol Soc Am Spec Pap 241, pp 101–126

Damm KW, Harmon RS, Kelley S (1994) Some isotope and geochemical constraints on the origin and evolution of the Central Andean basement (19–24°S). In: Reutter KJ, Scheuber E, Wigger PJ (eds) Tectonics of the Southern Central Andes. Springer Verlag, Berlin Heidelberg New York Tokyo, pp 263–275

DeWolf CP, Mezger K (1994) Lead isotope analyses of leached feldspars: constraints on the early crustal history of the Grenville Orogen. Geochim Cosmochim Acta 58: 5537–5550

Eckert JO, Newton RC, Kleppa OJ (1991) The ΔH of reaction and recalibration of garnet-pyroxene-plagioclase-quartz geobarometers in the CMAS system by solution calorimetry. Am Mineral 76: 148–160

Escayola M, Viramonte JG, Franz G, Becchio R, Popridkin MC, Arnosio M (1998) Los xenolitos de las rocas volcanicas alcalinas Cretacicas del sector sur de la sierra de Los Condores, Sierras Pampeanas de Cordóba, Argentina. X Congr Latinoamericano Geol, Buenos Aires, Actas (in press)

Evensen NM, Hamilton PJ, O'Nions RK (1978) Rare-earth abundances in chondritic meteorites. Geochim Cosmochim Acta 42: 1199–1212

Fowler CMR (1990) The solid Earth. Cambrigde Univ Press, Cambridge

Fowler CMR, Nisbet EG, Pandit BI (1988) The transfer of heat by conduction in the Earth's crust: physical constraints. In: Nisbet EG, Fowler CMR (eds) Short course on heat, metamorphism and tectonics, vol 14 Mineral Assoc Can, Short Course Handbook, pp 1–33

Fraga H, Introcaso A (1990) Un modelo gravimétrico litosférico para la subcuenca de Lomas de Olmedo (Cuenca del Norte y Noroeste) en la provincia Salta, Argentina. Rev Geofis Int 29: 89–99

Franz G, Lucassen F (1997) Upper Paleozoic crustal thickening – the basement of the Sierra de Limon Verde in N Chile (Region Antofagasta). VIII Congr Geol Chileno, Antofagasta, Chile, Actas Vol II: 1271–1274

Frost BR, Chacko T (1989) The granulite uncertainty principle: limitations on thermobarometry in granulites. J Geol 97: 435–450

Galliski MA, Viramonte JG (1988) The Cretaceous paleorift in northwestern Argentina; a petrological approach. J S Am Earth Sci 1: 329–343

Galliski MA, Yague AA, Risso C, Viramonte JG, Saavedra VA (1989) Contribución a la petrología y geoquimica de los xenolitos y basaltos alcalinos cretacicos de la quebrada de las Conchas, Provincia de Salta, Republica Argentina. Rev Asoc Argent Mineral Petrol Sedimental 20: 71–87

Goldstein SL, O'Nions RK, Hamilton PJ (1984) A Sm-Nd study of atmospheric dust and particulates from major river systems. Earth and Planet Sci Lett 70: 221–236

Graham CM, Powell R (1984) A garnet-hornblende geothermometer: calibration, testing and application to the Pelona Schist, Southern California. J Metamorphic Geol 2: 13–31

Green DH, Ringwood AE (1967) An experimental investigation of the gabbro eclogite transformation and its petrological applications. Geochim Cosmochim Acta 31: 767–83

Holdaway MJ (1971) Stability of andalusite and the aluminium silicate phase diagram. Am J Sci 271: 97–131

Holland T, Blundy J (1994) Non-ideal interactions in calcic amphiboles and their bearing on amphibole-plagioclase thermometry. Contrib Mineral Petrol 116: 433–447

Huang WI, Wyllie PI (1973) Melting relations of muscovite granite to 35 kbar as a model for fusion of metamorphosed subducted oceanic sediments. Contrib Mineral Petrol 42: 1–14

Ito K, Kennedy GC (1971) An experimental study of the basalt–garnet granulite–eclogite transition. In: Heacock JG (ed) The structure and physical properties of the Earth's crust. (Geophys Monogr, 14 Am Geophys Union) pp 303–314

Kay RW, Mahlburg Kay S (1993) Delamination and delamination magmatism. Tectonophysics 219: 177–189

Kay SM, Coira B, Viramonte J (1994) Young mafic back arc volcanic rocks as indicators of continental lithospheric delamination beneath the Argentine Puna plateau, central Andes. J Geophys Res 99 (B12): 24323–24339

Kay SM, Orrell S, Abbruzzi JM (1996) Zircon and whole rock Nd-Pb evidence for a Grenville age and a Laurentian origin for the basement of the Precordillera in Argentina. J Geol 104: 637–648

Köhler T, Brey GP (1990) Calcium exchange between olivine and clinopyroxene calibrated as a geothermobarometer for natural peridotites from 2 to 60 kbar with applications. Geochim Cosmochim Acta 54: 2375–2388

Kohn MJ, Spear FS (1990) Two new barometers for garnet amphibolites, with applications to southeast Vermont. Am Mineral 75: 89–96

Kretz R (1983) Symbols for rock-forming minerals. Am Mineral 68: 277–279

Lachenbruch AH, Morgan P (1990) Continental extension, magmatism and elevation; formal relations and rules of thumb. Tectonophysics 174: 39–62

Leake BE (1978) Nomenclature of amphiboles. Mineral Mag 42: 533–563

Lucassen F, Franz G (1997) Crustal recycling of metamorphic basement: Late Paleozoic granites of the Chilean Coast Range and Precordillera at 22°S. VIII Congr Geol Chileno, Antofagasta, Chile, Actas Vol II: 1344–1348

Lucassen F, Wilke HG, Viramonte J, Becchio R, Franz G, Laber A, Wemmer K, Vroon P (1996a) The Paleozoic of the Central Andes (18–26°S) – a metamorphic view (abstract). In: Third Int Symp Andean Geodyn Abstr Vol, St Malo, France, ORSTOM eds, Paris, pp 779–782

Lucassen F, Fowler CMR, Franz G (1996b) Formation of magmatic crust at the Andean continental margin during early Mesozoic: a geological and thermal model of the North Chilean Coast Range. Tectonophysics 262: 263–279

Lucassen F, Franz G, Laber A (1998) Permian high pressure rocks – the basement of Sierra de Limón Verde in N Chile. J S Am Earth Sci (in press)

Marquillas RA, Salfity JA (1988) Tectonic framework and correlations of the Cretaceous-Eocene Salta Group; Argentina. In: Bahlburg H, Breitkreuz Ch, Giese P (eds) The Southern Central Andes. (Lecture notes in Earth sciences, 17) Springer Verlag, Berlin Heidelberg New York Tokyo, pp 119–136

Mezger K, Essene EJ, Halliday AN (1992) Closure temperatures of the Sm-Nd system in metamorphic garnets. Earth Planet Sci Lett 113: 397–409

Morimoto N (1989) Nomenclature of pyroxenes. Can Mineral 27: 143–156

Omarini RH, Götze HJ (eds) (1991) Global geoscience transect 6: Central Andean transect, Naszca Plate to Chaco plains, southwestern Pacific Ocean, Northern Chile and Northern Argentina. Publ Int Lithosphere Program, Am Geophys Union, Washington

Perchuk LL, Aranovich LY, Podlesski KK, Lavranteva IV, Gerasimov VY, Fedkin VV, Kitsul VI, Karsakov LP, Berdnikov NV (1985) Precambrian granulites of the Aldan shield, eastern Siberia, USSR. J Metamorphic Geol 3: 265–310

Richard P, Shimizu H, Allègre CJ (1976) $^{143}Nd/^{146}Nd$, a natural tracer: an application to oceanic basalts. Earth Planet Sci Lett 31: 269–278

Risso C (1990) El volcanismo del tramo superior de la quebrada del rio Las Conchas, departamentos La Viña, Guachipas y Cafayate, Provincia de Salta (unpublished). PhD thesis, Univ Buenos Aires, Argentina

Risso C, Viramonte JG (1992) Xenolitos de lerzolitas espinelicas piroxenitas y granulitas como herramientas de la aproximacion en la modelzacion de la litosfera precretacica del noroeste Argentino, Qda de Las Conchas, Salta. I Reunion Mineral Metal, I Jornadas Mineral Petrogr Metal Rocas Ultrabasicas, La Plata Argentina, Actas (2): 449–463

Rudnick RL, Presper T (1990) Geochemistry of intermediate- to high-pressure granulites. In: Vielzeuf D, Vidal Ph (eds) Granulites and crustal evolution. Kluwer Academic Dordrecht, Publishers, pp 523–550

Salfity JA, Marquillas RA (1994) Tectonic and sedimentary evolution of the Cretaceous–Eocene Salta Group basin, Argentina. In: Salfity JA (ed) Cretaceous tectonics of the Andes. Vieweg Braunschweig, pp 266–315

Shaw CSJ, Edgar AD (1997) Post-entrainment mineral-melt reactions in spinel peridotite xenoliths from Inver, Donegal, Ireland. Geol Mag 134: 771–779

Stacey JS, Kramers JD (1975) Approximation of terrestrial lead isotope evolution by a two-stage model. Earth Planet Sci Lett 26: 207–221

Thöni M, Jagoutz E (1992) Some new aspects of dating eclogites in orogenic belts: Sm-Nd, Rb-Sr, and Pb-Pb isotopic results from the Austroalpine Saualpe and Koralpe type-locality (Carinthia/Styria, southeastern Austria). Geochim Cosmochim Acta 56: 347–368

Tosdal RM (1996) The Amazon-Laurentian connection as viewed from the Middle Proterozoic rocks in the central Andes, western Peru and northern Chile. Tectonics 15: 827–842

Toselli A, Rossi de Toselli J, Rapela C (1978) El basamento metamórfico de la Sierra de Quilmes, República Argentina. Rev Asoc Geol Argent 33: 105–121

Viramonte JG, Kay SM, Noviski I, Becchio R, Escayola M (1998) Cretaceous rift related magmatism in south-central south America. J S Am Earth Sci (in press)

Wells PRA (1980) Thermal models for the magmatic accretion and subsequent metamorphism of continental crust. Earth Planet Sci Lett 46: 253–256

White RS, McKenzie D (1989) Magmatism at rift zones: the generation of volcanic continental margins and flood basalts. J Geophys Res 94: 7685–7729

Wigger PJ, Schmitz M, Araneda M, Asch G, Baldzuhn S, Giese P, Heinsohn WD, Martinez E, Ricaldi E, Rüwer P, Viramonte J (1994) Variation in the crustal structure of the southern central

Andes deduced from seismic refraction investigations. In: Reutter KJ, Scheuber E, Wigger PJ (eds) Tectonics of the southern central Andes. Springer Verlag, Berlin Heidelberg New York Tokyo, pp 23–48
Wyllie PJ (1992) Experimental petrology: earth material science. In: Brown GC, Hawkesworth C, Wilson C (eds) Understanding the Earth. Cambridge Univ Press, Cambridge, pp 67–87
York D (1969) Least squares fitting of a straight line with correlated errors. Earth Planet Sci Lett 5: 320–324
Zuleger E, Erzinger J (1988) Determination of REE and Y in silicate materials with ICP-AES. Fresenius Z Anal Chem 332: 140–143